Physical Origin of a Wet Microburst: Observations and Theory

DAVID ATLAS

NASA Goddard Space Flight Center, Greenbelt, Maryland

CARLTON W. ULBRICH

Department of Physics and Astronomy, Clemson University, Clemson, South Carolina

CHRISTOPHER R. WILLIAMS

University of Colorado and NOAA Aeronomy Laboratory, Boulder, Colorado

(Manuscript received 16 June 2003, in final form 25 November 2003)

ABSTRACT

A unique set of Doppler and polarimetric radar observations were made of a microburst-producing storm in Amazonia during the Tropical Rainfall Measuring Mission (TRMM) Large-Scale Biosphere–Atmosphere (LBA) field experiment. The key features are high reflectivity (50 dBZ) and modest size hail (up to 0.8 mm) in high liquid water concentrations (>4 g m^{-3}) at the 5-km 0°C level, melting near the 3-km level as evidenced by the Doppler spectrum width on the profiler radar (PR), by differential polarization on the S-band dual-polarized radar (S-POL), and a sharp downward acceleration from 2.8 to 1.6 km to a peak downdraft of 11 m s^{-1}, followed by a weak microburst of 15 m s^{-1} at the surface. The latter features closely match the initial conditions and results of the Srivastava numerical model of a microburst produced by melting hail. It is suggested that only modest size hail in large concentrations that melt aloft can produce wet microbursts. The narrower the distribution of hail particle sizes, the more confined will be the layer of melting and negative buoyancy, and the more intense the microburst. It is hypothesized that the timing of the conditions leading to the microburst is determined by the occurrence of an updraft of proper magnitude in the layer in which supercooled water accounts for the growth of hail or graupel.

1. Introduction

The present study is based upon a major field campaign [Tropical Rainfall Measuring Mission–Large-Scale Biosphere–Atmosphere Experiment (TRMM–LBA)] that took place in the Rondonia region of the Brazilian Amazon. The storm under discussion occurred on 17 February 1999 and has been discussed by Atlas and Williams (2003a,b, hereafter AWa and AWb), and Williams and Rutledge (2003, manuscript submitted to *Mon. Wea. Rev.*, hereafter WR). Rickenbach et al. (2002) have studied the large-scale synoptic conditions responsible for the transient frontal systems in the region during the interim periods of easterly and weak westerly flow. They have shown that mesoscale convective systems (MCS) in easterly regimes are more vigorous and produce more rainfall than those in westerly conditions. Williams and Rutledge focused upon the kinematic, microphysical, and latent heating features in one MCS in each regime. Their study of the case of 17 February in the easterly regime provides a broader context for the conditions that set the stage for the microburst studied here.

Atlas and Williams (AWa) addressed the microphysics and flow field that occurred during the 17 February storm. They found that the precipitation that occurred in the early stage of the storm originated as warm rain and was characterized by an equilibrium drop size distribution. Also the later precipitation was in the form of graupel or hail that had formed in the upper reaches of the updraft. It was during the latter stage that lightning activity increased sharply, a finding that was elaborated in AWb. Finally, they also noted the occurrence of the microburst discussed here and its possible origin. The thrust of the present paper is to characterize the nature of the microburst in detail and to provide the physical reasons for its occurrence.

The microburst noted in AWa passed directly over the profiler radar (PR), thus making it possible to observe its characteristics in unprecedented detail. The burst occurred at the end of a period of intense rain resulting from melting of hail. The PR shows the antecedent microphysics and the downward acceleration

Corresponding author address: Dr. David Atlas, NASA Goddard Space Flight Center, Code 910, Greenbelt, MD 20771.
E-mail: datlas@radar.gsfc.nasa.gov

of the air while the surface observations show the wind shift and gust front. The interpretation of these events is aided by a prior numerical simulation by Srivastava (1987). The nature and origin of microbursts has also been treated by Fujita (1985) and Proctor (1988, 1989), among others, and thoroughly reviewed by Wakimoto (2001). This is a case of a ''wet'' microburst; that is, one that occurs with heavy precipitation as opposed to a ''dry'' one that occurs as a result of evaporation of light precipitation. Only this event and that reported by Wakimoto and Bringi (1988) have been observed with sufficient accompanying microphysical data to provide a robust physical interpretation.

2. Observations

a. Surface data

Figure 1 presents the surface observations at the location of the PR for the entire hour starting at 1700 UTC (all times in UTC). (The reflectivity pattern and associated dual-Doppler wind field are presented later in Fig. 5.) The initial temperature and relative humidity (RH) are 30.4°C and 62%. With the onset of precipitation the RH increases rapidly to more than 80% and remains at such higher levels during the passage of the storm. Likewise, the temperature drops rapidly to about 24°C as precipitation starts and remains at about this lower value. The wind picks up with the onset of rain at about 1707 but remains SE until 1722. At that time it shifts to N at about 1725 and weakens until the gust of 15 m s^{-1} hits at 1732. These observations are consistent with the occurrence of a microburst at the surface. The peak gust of 15 m s^{-1} is in the lower range of bursts reported by Wakimoto (2001).

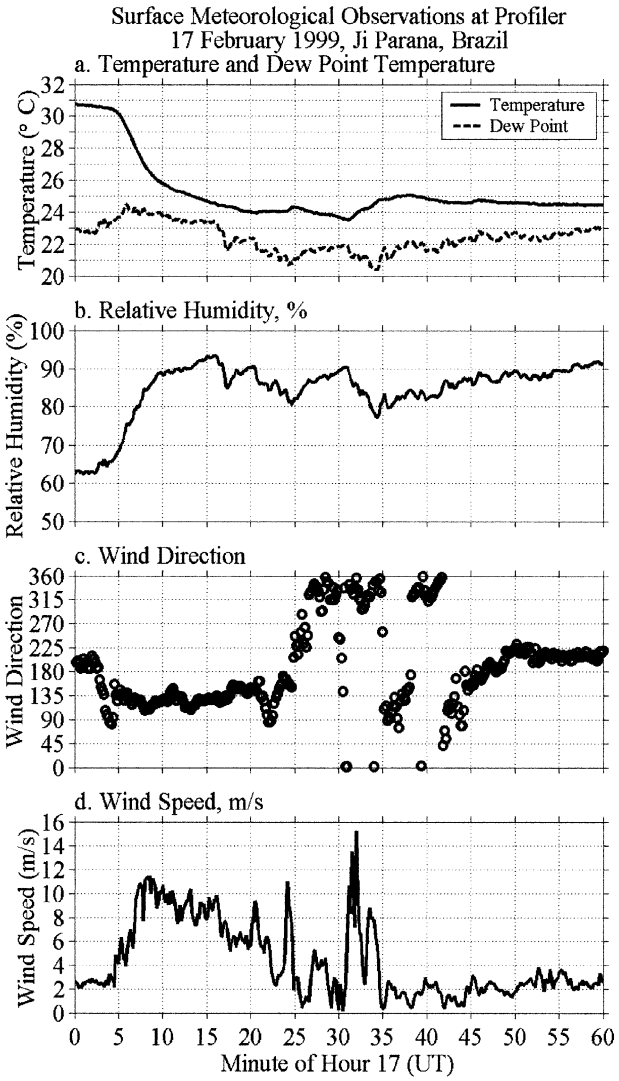

FIG. 1. Surface meteorological parameters for hour starting at 1700 UTC 17 Feb 1999 at Parana: (a) Temperature, (b) relative humidity, (c) wind direction, and (d) wind speed. Note wind shift starting at 1728 and peak gust denoting the microburst.

b. Sounding

Figure 2 shows a sounding of the atmosphere at Rebio Jaru, Brazil, which is located 80 km to the north of the profiler. The 1500 UTC sounding was chosen because it is believed to be most representative of the conditions at the profiler location 2 to 2.5 hours later, the time of interest. No soundings were taken at the profiler. It is seen that the 0°C level occurs at 4.7 km and the lifting condensation level is at 2 km. From these data the sounding suggests that storm cloud top would reach levels in excess of 10 km. Winds are light and variable (less than 5 m s^{-1}) in the altitudes below 4 km and attain speeds near 10 m s^{-1} in the mid levels (5–10 km). Note that the winds above 10 km are strong and from the east. This is consistent with the satellite observations that show the storm anvil extending toward the west (not shown). At almost all levels the winds have a predominantly easterly component; however the storm itself was moving from the NNE. The convective available potential energy (CAPE) for this sounding is 1683 J kg^{-1} and the CIN (convective inhibition) is only 3 J kg^{-1}, thus indicating an atmosphere that is moderately unstable.

The inset diagram shows the sounding of relative humidity up to 10 km. Note that the RH in the mid levels from about 3 to 7 km varies between 60% and 70%. This fact will be useful later in comparing the observational data to the theoretical model of a microburst.

c. Profiler observations

1) 1726 UTC

The profiler was located at Ji Parana (see WR for a map of the distribution of instruments in the LBA area). Figure 3 shows the PR profile of the Doppler spectra at 1726. The reflectivity spectral density [dBZ (m s^{-1})$^{-1}$] is

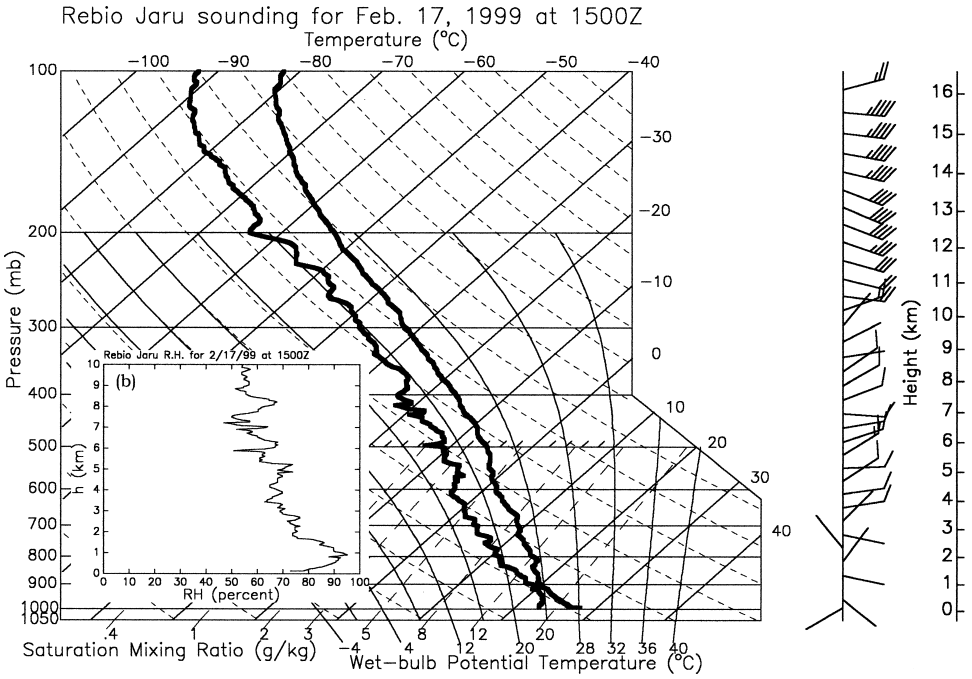

FIG. 2. The sounding at Rebio Jaru at 1500 UTC. Wind barbs are in m s^{-1}, long barbs are representative of 5 m s^{-1}. The inset figure shows the relative humidity vs altitude up to 10 km.

shown by the color bar at the right. The white line corresponds to $\langle V \rangle$, the mean Doppler velocity. The vertical profile of total reflectivity is shown to the left of the color bar. The 0°C level is at 5 km. There is no bright band (BB) at this time or on any of the profiles during the previous 15 min, and the linear depolarization ratio (LDR) was zero on the S-band dual-polarized polarimetric radar (S-POL). This indicates the absence of snow. Instead the Z profile corresponds to that expected for melting hail (AWa). (S-POL was located at 42 km and 203° from the PR.)

The maximum downward velocity is 24 m s^{-1} at a height of 1.6 km. The acceleration begins at 2.8 km where the maximum downward velocity is 13 m s^{-1}. Assuming no change in the broadening of the spectrum due to turbulence between 2.8 and 1.6 km, the net increase is 11 m s^{-1}. Alternatively we may use the difference in $\langle V \rangle$ at the two levels: 7 and 17 m s^{-1}, respectively, or 10 m s^{-1}. Thus the average downdraft is about 10 to 11 m s^{-1}. The average of the total speed (air plus particles) of fall in this 1.2-km-deep layer is 12 m s^{-1}, thus taking 100 sec. The acceleration is then $\Delta\langle V \rangle/\Delta t \approx 0.1$ m s^{-2}. The divergence is $\Delta V/\Delta h \approx -0.08$ s^{-1}.

In the five PR profiles between 1723:00 and 1725:00 (not shown), there is no evidence of significant updrafts between 2 and 5.5 km. At 1725 there is no updraft below 3 km and $\langle V \rangle \approx 8$ m s^{-1} in the 2.2-km–2.8-km layer. Thus there is no reason to doubt the above estimate of the downward acceleration.

The lower bound of the Doppler spectra at the 0°C level during the period 1724–1726 is zero, thus indicating the absence of any updraft there (Battan 1964). Using the single Doppler S-POL range height indicator (RHI) at 1728 we prepared a qualitative picture of the streamlines in vertical cross section over the profiler (not shown). This picture showed that the updraft below the 6-km level had decayed in the vicinity of the profiler while the draft was maintained at the upper levels. Thus there is good evidence for the absence of any updraft at the 5-km level near the time of the microburst.

The upper bound of the Doppler spectrum in Fig. 3 is 16 m s^{-1} at the 0°C level. Assuming no spectral broadening due to other factors, this corresponds to a maximum diameter of 0.83 cm based upon the fall speed law for hail due to Douglas (1964) and the correction to sea level due to Beard (1976). In order to correct for possible spectrum broadening we make the arbitrary assumption that the portion of the variance of the Doppler spectrum due to factors other than the fall speed spectrum is 0.5 of the total variance. Under this assumption the upper bound of the fall speed spectrum alone (say at 2 sigma) is 14.8 m s^{-1}. The latter value corresponds to a maximum hail diameter of 0.70 cm. Thus the probable range of maximum hail diameters is between 0.70 and 0.83 cm. Such hail would melt completely in a fall of 5 km to the surface at a temperature of 28°C and relative humidity of 0.73 as observed in the sounding at Rebio Jaru in Fig. 2 (Rasmussen and Heymsfield 1987a). There was no hail observed in the vicinity of the profiler.

The decrease in the downward mean Doppler velocity

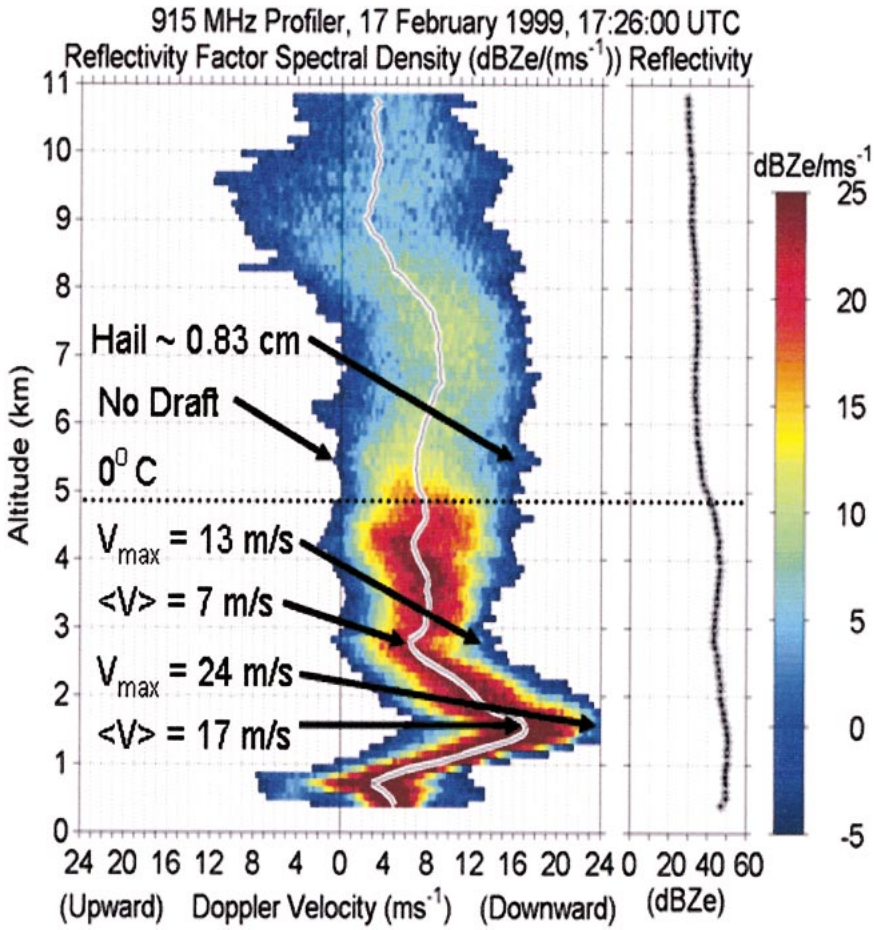

FIG. 3. Profiler Doppler spectra vs height with 100-m vertical resolution. Doppler spectral density [dBZ (m s^{-1})$^{-1}$] shown by the color bar at right. Profile of total reflectivity is between the color bar and the profile. Arrows point to individual features discussed in text.

below the 1.6-km level is consistent with the divergence of the downdraft that must occur as the air approaches the surface (Wakimoto 2001, Fig. 7.12).

2) TIME–HEIGHT RECORD

A time–height record of Z, $\langle V \rangle$, and Doppler spectrum width (SW) is shown in Fig. 4. A similar record is shown in AWa. While our discussion of these records imply an assumption of steady state, we have used the S-POL radar observations to infer some of the changes with time. However, Fig. 4 is presented to display the internal structure in greater resolution. The 0°C level is shown at a height of 4.7 km based upon the sounding. However, the vertical profiles of total reflectivity (as in Fig. 3) show a systematic downward increase at heights of 5.0 to 5.2 km. Such an increase is due to wetting of the surface of the hail, thus indicating that the 0°C level within the storm is slightly higher than that shown by the sounding.

Figure 4a indicates that the reflectivity ranges between 40 and 50 dBZ up to the 5-km level between 1710 and 1730. These large Z values continue aloft for another 6 min. Note that there is no bright band near the 0°C level throughout this period. The sudden end of the large Z at the surface is consistent with the sharp end of the rain measured by the disdrometer. Also, note the maximum $Z > 50$ dBZ between 1725 and 1727 and height 0.8 to 1.6 km. This corresponds closely to the time at which the surface mass-weighted drop size attains a peak of 3.1-mm diameter and disdrometer-based values of Z also exceed 50 dBZ (AWa).

Figure 4b presents the record of mean Doppler velocity $\langle V \rangle$. The tilted column of light green (and other colors within the light green) represents the updraft. Here $\langle V \rangle$ increases to a maximum of $+18$ m s^{-1} at 11 km; however, the lower bound of the Doppler spectrum, representing the updraft velocity, is $+24$ m s^{-1}. The updraft passes through the 0°C level at about 1712. Assuming a mean raindrop fall speed of $\sim$8 m s^{-1}, the time of fall from 5 km is $\sim$10 min. Hence all the rain occurring at the surface prior to about 1720 has been generated by means of warm processes such as collision, coalescence, and breakup (CCB). In AWa we showed

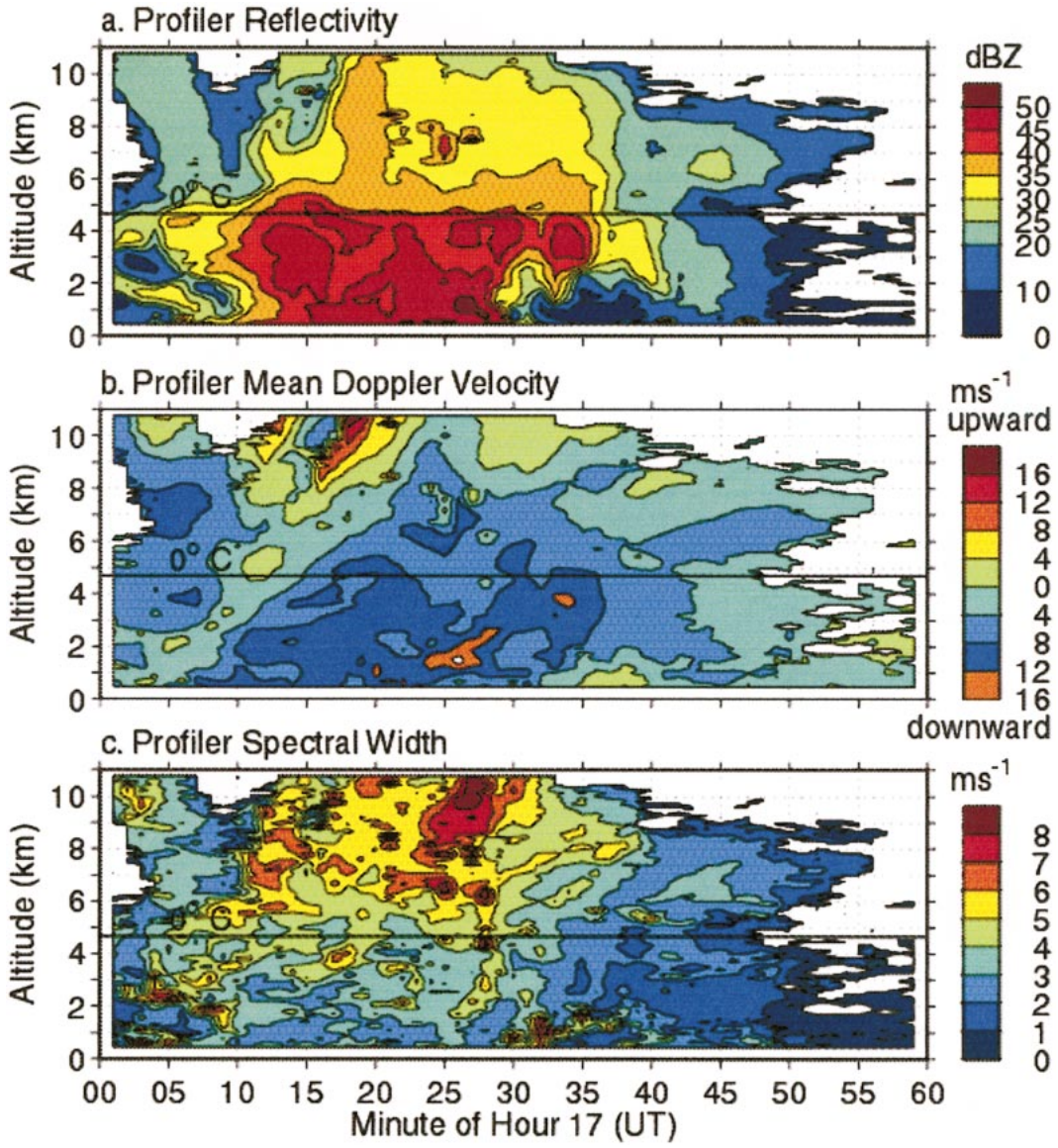

FIG. 4. (a) Profiler time–height record of dBZ, (b) mean Doppler velocity, and (c) Doppler spectrum width for the hour starting at 1700 UTC 19 Feb 1999.

that prior to 1712, the time at which the updraft passed through the 0°C level, there was a balance layer (i.e., where $\langle V \rangle \approx 0$) between 3 and 5 km. This suspends the midrange of drop sizes and extends the period of warm drop growth to produce an equilibrium drop size distribution (Hu and Srivastava 1995; Atlas and Ulbrich 2000). This, in turn, is responsible for the nearly linear relation $Z = 1260R^{1.04}$ between radar reflectivity Z and rain rate R.

Those drops that have fall speeds less than the updraft at the balance level continue to rise. They must freeze to form graupel and hail. However, a penetration of the storm cell at the −18°C level between 1810 and 1812 (subsequent to the storm's weakening) by the Citation aircraft carrying a cloud particle imager showed a variety of ice crystal types: tiny frozen drops of 30- to 60-μm plates, capped columns, aggregates up to 0.75 mm, and tiny graupel up to 0.4 mm (Stith et al. 2002). In the updraft of 8 to 9 m s^{-1} at the 5-km level at 1712 (during the vigorous portion of the storm) the largest drops that rise are about 2 mm in diameter. These would freeze and continue to grow by riming and/or the collection and freezing of the supercooled water in the updraft, which continues to increase with height. We have seen from Fig. 3 that we must have maximum size hail of about 0.7–0.8 cm diameter at 1726. The maximum downward speeds seen by the profiler suggest equal or larger hail during the previous 15 min. We shall see that the storm has decayed substantially between 1712 and the aircraft penetration at 1810. Also, all pilots

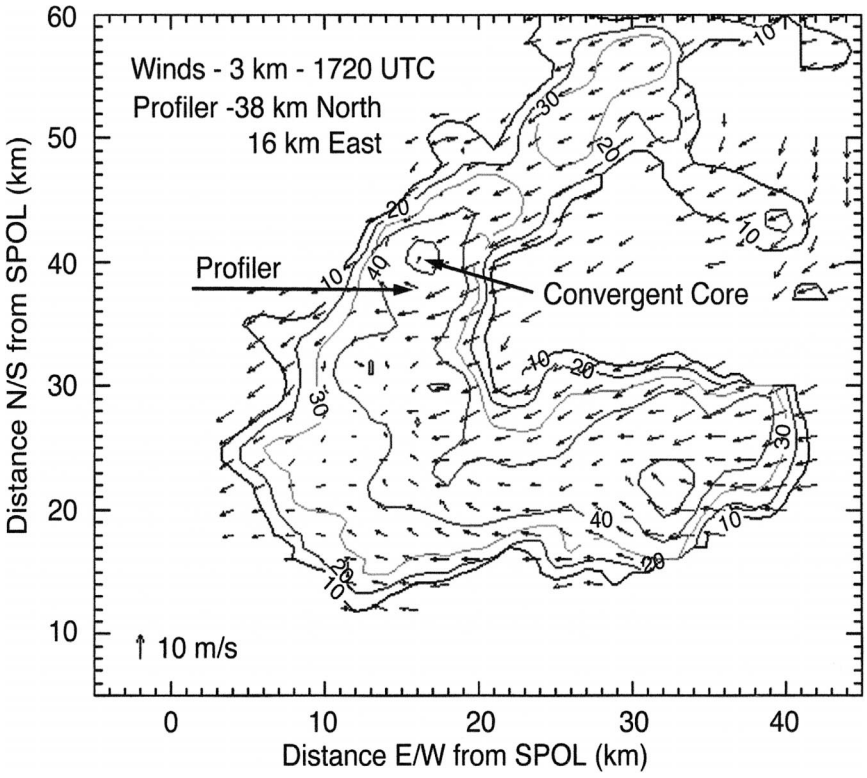

FIG. 5. Dual Doppler winds at the 3-km level at 1720 UTC 19 Feb 1999. Note scale of wind barbs at lower left. Positions of the center of convergence and the profiler are also shown. Contours represent reflectivity in 10-dB*Z* intervals.

tend to avoid the storm cores so that it is no surprise that the Citation did not observe the somewhat larger hail and graupel that we believe must have been present.

In Fig. 4b the white spot at 1.6 km and 1726 indicates a maximum downward $\langle V \rangle$ greater than 16 m s^{-1}. This corresponds to the maximum $\langle V \rangle$ in the 1726 profiler record of Fig. 3 and the maximum *Z* in Fig. 4a. This point is just below the minimum height of the V-shaped pattern of the 8 m s^{-1} isopleth. This V-shape is mindful of the bow-shaped echoes that characterize circulations in horizontal displays of severe storms and squall lines. This, and the corresponding downward displacement of the 45-dB*Z* isopleth in (a) suggests a downdraft that we have seen in Fig. 3. Later (Fig. 5) we shall show that this region is marked by convergence in the horizontal wind field.

Figure 4c shows the Doppler spectrum width (SW), that is, the standard deviation of the spectrum. The most prominent feature is the sharp decrease in SW from values >5 to <4 m s^{-1} from 6 to 4.5 km, just below the 0°C level. In the period 1710 to 1722, SW decreases from 4–5 m s^{-1} above 3 km to 2–3 m s^{-1} below. This is consistent with the decrease in the fall speed of the larger hail or graupel due to melting and the shedding of the melt water into rain. However, values of 2–4 m s^{-1} are still greater than that attributable to rain alone, even of rates of 100 mm h^{-1} (Atlas et al. 1973) or values computed for this storm from surface disdrometer data. The excess is attributable to a combination of turbulence and crosswind air motion across the 6.5° beam width of the profiler.

Figure 3 also shows that the lower bound of the Doppler spectrum is considerably larger than zero in the altitude range from about 2.5 down to about 1 km. Between 2.5 to 1.5 km the lower bound increases continuously and the entire Doppler spectrum is shifted to larger velocities. This clearly demonstrates that the vertical winds and the precipitation particles carried along by such winds are accelerating downward as discussed above.

d. S-POL radar observations

DUAL DOPPLER WINDS

Figure 5 shows the dual Doppler winds at the 3-km level at 1720.[1] The center of convergence at this level is just 2 km northeast of the PR. Six minutes later at the time of the peak downdraft viewed by the PR the convergence center should be even closer to the PR since the storm cell is moving toward the SSW (AWa).

[1] This figure was provided by A. Williams, formerly of the Department of Atmospheric Sciences, Colorado State University.

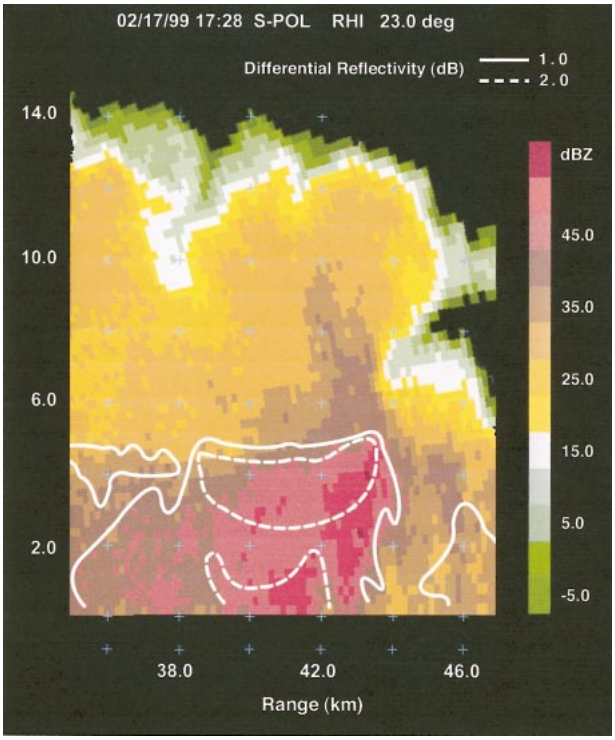

FIG. 6. S-POL radar vertical cross section at 23° azimuth over the profiler located at 42-km range. Only the section between 37 and 47 km is shown. The reflectivity (dBZ) is shown in color according to the color bar at right; for example, the 45-dBZ color represents the range of 40 to 45. The white contours represent differential reflectivity (Z_{DR}); solid is 1 dB; dashed is 2 dB.

A convergence center is also evident at the 7-km level (not shown) but it is displaced 2 km south of that at 3 km. Because the wind vectors are plotted at 2-km spacing, one can only make a crude estimate of the convergence at this level. It is $\sim 0.005\ s^{-1}$. This is more than an order of magnitude smaller than the vertical divergence deduced from the PR observation in Fig. 3 ($\Delta V/\Delta h \approx -0.08\ s^{-1}$). Dual Doppler cross section of the winds in the 23° azimuth plane over the PR and 1 km to either side of that plane made at 1730 (not shown) failed to show any evidence of the convergence or the microburst at that time. This suggests that the microburst is a small, short duration event.

Figure 6 presents a vertical cross section taken at 1728 with the S-POL radar pointing at 23° azimuth directly over the profiler located at 42-km range. This cross section covers the range between 35 and 47 km. The left side is at the SSW end. The colors represent the reflectivities according to the color bar at the right. The cell between 38 and 44 km is the one that passed over the profiler between 1700 and 1728. In the next few minutes the cell completed its passage over the profiler. One notes an excellent correspondence in the reflectivities measured by both radars, the top of the high reflectivity region just below the 5-km level, the absence of a bright band, and the structure of the NNE side with an overhanging high reflectivity region. At this time the cell has weakened somewhat relative to that at 1711 (see AWa).

The solid and dashed white isopleths in Fig. 6 correspond to differential reflectivity (Z_{DR}) of 1 and 2 dB, respectively. Because the Z_{DR} patterns were noisy it was necessary to use some judgment to analyze each region with reasonable confidence. These regions would correspond to mass-weighted drop diameters $D_m = 1.8$ and 2.3 mm, respectively, if the Z_{DR}–D_m relation of Bringi et al. (2002) were used. However, the proximity of these regions to the 0°C level, the absence of a bright band, and evidence of hail or graupel raised doubts that we would find such large raindrops in this layer. On the other hand, the work of Rasmussen and Heymsfield (1987b) demonstrates that hail tends to melt while retaining an oblate coating of water. Hence the melting particles act like horizontally oriented oblate raindrops. Vivekanandan et al. (1990) have computed the various polarimetric properties of *individual* melting hail and graupel particles such as that proposed by Rasmussen and Heymsfield and found that values of Z_{DR} reach 4 dB for hail of initial diameter of 6 mm. Nevertheless, the average sizes cannot be determined without knowledge of the initial size distribution. We have also examined the S-POL vertical cross sections in the 23° plane over the PR at 1718:29 (not shown). These show Z_{DR} up to 2.5 dB between the 2- and 4-km level, also believed to be due to melting hail or graupel. (The reader will find further discussion and observations of melting particles in Bringi and Chandrasekar 2001, 451–458.)

For present purposes, however, it suffices to know that the regions of differential reflectivity below the 0°C level correspond to melting hail or graupel. Moreover, the base of the 2-dB isopleth of Z_{DR} evidently represents the region at which a significant, if not major, fraction of the melting is complete. This is found at a height of 2.5 km, in reasonable agreement with the altitude that we have previously deduced from the narrowing of the Doppler spectrum width. Regarding the occurrence of a U-shaped region of Z_{DR} of 2 db below the 2-km level, we suggest that this does represent mass-weighted diameters of 2.3 mm, in good agreement with that computed from the surface drop size distribution (see AWa). Their occurrence here may be due to the water shed from the melting hail. It is also possible that a sheath of larger drops has entered the observational plane below the 2-km level from the side. Values of the median volume diameter (D_0) and rain rate (R) within ± 0.5 km in range and slightly above the PR deduced from the S-POL radar are $D_0 = 2.05$ mm and $R = 117$ to 144 mm h^{-1} (V. N. Bringi 2003, personal communication). These are in good agreement with values measured directly by the disdrometer (see AWa).

3. Comparison to theory

These and other features of the profiler records are in very good agreement with the theoretical predictions

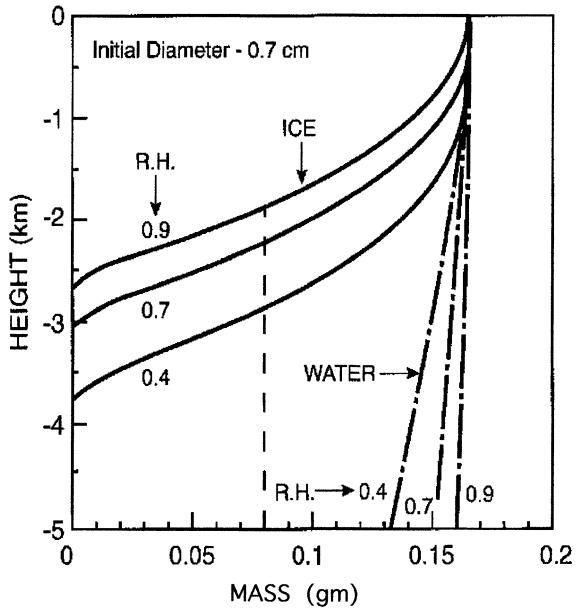

FIG. 7. Mass of an evaporating water drop and of ice in a melting ice particle as a function of height below the 5-km level in an atmosphere of the relative humidity shown and lapse rate 7 K km^{-1}. Initial diameter is 7 mm. The dashed vertical line corresponds to 50% loss of mass (after Srivastava 1987).

of Srivastava (1987) for a downdraft driven by melting and evaporation of precipitation. The theory assumes that ice particle spheres start at a given level completely frozen and melt during their descent while retaining their spherical shapes and the melted water; that is, no liquid water is shed during the fall. Both solid hail and graupel are considered in the model and various values of the environmental relative humidity are used in the calculations. Srivastava shows that the melting of ice proceeds slowly at first during its fall, probably due to sublimation especially when the relative humidity is low (less than about 0.50). However, after falling by only about 1–2 km (depending on the value of RH), the melting proceeds very rapidly. For example, an ice particle that melts completely in a fall through about 3 km at RH = 0.4 needs to fall only 2 km at RH = 0.9. This difference is due to the release of latent heat in the latter case from the greater condensation of water vapor on the melting ice particle surface. The initial conditions used by Srivastava in his model are that the particle starts at a pressure of 550 mb (altitude of about 5.1 km for the storm considered here) where the temperature is 0°C. The lapse rate of environmental temperature is assumed to be 7.0 K km^{-1}. These environmental conditions are very similar to those for the LBA storm studied in this work.

Figure 7 shows the results of calculations by Srivastava for the melting and evaporation of ice particles and water drops with an initial diameter of 0.7 cm. This initial value of the particle diameter is very similar to that deduced above from the profiler Doppler spectra in the altitude range 5–6 km. Each of the curves for ice and water is labeled with the values of RH assumed in the calculations. The sounding acquired at Rebio Jaru for the time of the storm indicates that the RH in the altitude range 3 to 5 km (or in the 2 km below the assumed starting point) is roughly constant varying between about 0.6 and 0.7. However, in the precipitation area under study the RH is likely to be even greater than 0.7 and the rate of melting somewhat larger than that at lesser humidity. The dashed line in Fig. 7 corresponds to a reduction of ice particle mass to 50% of its initial value. From Fig. 7, the curves for RH = 0.7 show that the mass of the liquid water drop is reduced very little by evaporation during its fall, whereas the mass of an ice particle is decreased by 50% during a fall of about 2.2 km. It is notable that the remaining 50% of the ice melts in a layer only 0.8 km thick. Therefore, the latent heat of melting used is concentrated in a shallow layer near the height at which the particle is completely melted. It is clear from these calculations that the higher the RH, the faster the ice particles melt, whereas there is little effect with either altitude or RH on the mass of the liquid water drops. This has been explained in the previous paragraph as being due to the greater condensation of water vapor on the melting ice particle. The fact that the latent heat extracted from the atmosphere is concentrated in a shallow layer means that the lower layers are more negatively buoyant than those above, which would produce a downward acceleration, in agreement with profiler observations. This is especially true for the case of melting ice particles for which the temperature of the surface of the water coated particle remains close to 0°C during melting. The temperature difference between the ambient environment and the ice-cooled air increases as the particles descend, thus producing strong negative buoyancy.

The effects of these microphysical processes on the behavior of the downdraft have been calculated by Srivastava (1987) using the initial environmental conditions specified above. In addition, he assumed that the initial size distribution of frozen particles is of Marshall–Palmer form with slope equal to 17 cm^{-1} and intercept of 0.08 cm^{-4}. The precipitation mixing ratio at the top of the downdraft was assumed to be 3.9 g kg^{-1} and the reflectivity factor was taken to be 49 dB*Z*. The latter value is in good agreement with that measured at an altitude of 5 km by the profiler as well as the S-POL radar. The mixing ratio value agrees well with that determined from disdrometer data at the earth's surface.

Figure 8 (left) shows the results of the calculations for the downdraft velocity as a function of height and at 100-s intervals; Fig. 8 (right) shows the buoyancy at the same times [buoyancy = $(T_d - T_e)/T_e$, where T_d and T_e are the virtual temperatures of the downdraft and environment, respectively]. It is seen that the peak downdraft descends and increases with time until it reaches a maximum value of about 11 m s^{-1} at 300 s and at an altitude of 2 km below the 5-km starting height.

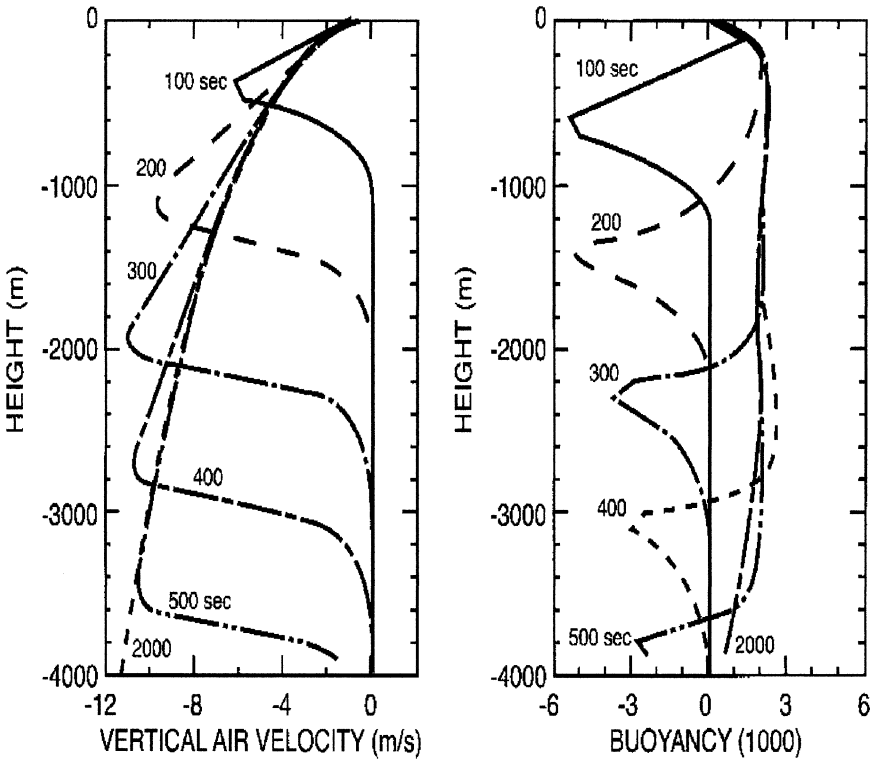

FIG. 8. (left) The vertical velocity and (right) buoyancy (×1000) resulting from the melting of an exponential distribution of ice particles with slope of 17 cm^{-1}, intercept of 0.08 cm^{-4}, mixing ratio of 3.9 g kg^{-1}, and reflectivity of 49 dBZ at the starting height of 5 km. Lapse rate is 7.0 K km^{-1}. Heights are below the 5-km level (after Srivastava 1987).

This value of the peak downdraft is remarkably close to that deduced from the 1726 profiler record in Fig. 3. It is also seen that the negative buoyancy is concentrated in a layer just below the depth to which the downdraft has penetrated at that time. After about 2000 sec the model reaches a steady state with a uniformly increasing downward velocity and a small positive buoyancy throughout the column. From these results it may be concluded that in the early stages the downdraft is driven by the negative buoyancy provided by the melting ice particles and eventually in the steady state by the combined effects due to melting and the weight of the descending precipitation. For the storm considered in this work, the steady state is not observed (and was probably not achieved at later times) since it is apparent that the event was transient and of short duration.

It may be concluded from this discussion of the theory and observations that the storm studied here involved a relatively weak, small-scale, short-lived microburst that was driven by the melting of hail formed above 5-km altitude with initial diameter in the 0.7–0.8-cm range. The negative buoyancy produced was due to the combined effects of melting and the weight of the descending precipitation.

A most intriguing question concerns the reasons for the limited time–space scale for the occurrence of the microburst. Here we can only speculate. In order to grow hail (or graupel) we require the presence of supercooled water. This is rarely to be found at very cold temperatures, say below about −20°C. In addition, in order to grow hail to about 0.7–0.8-cm diameter we require that the updraft in the supercooled water region reach values of about 8 to 10 m s^{-1}. Thus, we examined the profiler for the existence of a lower bound of the Doppler spectrum (i.e., approximately the value of the updraft) in the region likely to contain supercooled water. We found that the tilted updraft having values in excess of 8 to 10 m s^{-1} occurred in the height range of 6 to 8 km, corresponding to a temperature range of −5° to −18°C, between 1715 and 1719 (not shown). The updraft increased sharply above the 8-km level, presumably due to the unloading of the hail. Lighting activity also increased suddenly at 1715 indicating the presence of hail in the balance layer where charging and charge separation is likely to occur (AWb). The Profiler record of Fig. 4 shows that the start of the lowering of the high reflectivity (Fig. 4a) and large mean fall speed (Fig. 4b) region near the 5-km level started at ~1720. The falling of these zones terminated almost exactly at 1726, the time of the microburst on the profiler. It therefore appears that it is the combination of the drafts and the microphysics in the right altitude/temperature zone that was responsible for the initiation of the microburst. It is unlikely that the microburst continued further to the

SSW since the S-POL radar indicated that the storm cell dissipated after passing over the profiler. We emphasize that this explanation is speculative and requires further examination.

4. Summary and conclusions

The onset of the wet microburst was first observed by the 915-MHz profiler radar (PR) and subsequently by the wind shift and 15 m s^{-1} gust at the surface. Here we summarize the kinematic and microphysical features associated with and responsible for the microburst as observed by both the PR and the polarimetric S-POL radar. Although the event was a weak category burst, the observations are unique and provide substantial physical insight into their origin.

The features of the burst observed by the PR are

- a sharp downward acceleration of the vertical velocity between the 2.8- and 1.5-km levels;
- indications of no change with height of that portion of the mean Doppler velocity due to the fall speed of the particles;
- estimates of the downward acceleration of the air between 2.8 and 1.6 km by a net of 10–11 m s^{-1}, followed by the wind shift and gust of 15 m s^{-1} at the surface.

The information that contributes to our understanding are

- the absence of a bright band and a reflectivity profile characteristic of hail or graupel;
- the absence of an updraft immediately above the 0°C level allowing us to estimate the maximum hail size from the upper bound of the Doppler spectrum as 0.7–0.8 cm;
- the downward decrease of the width of the Doppler spectrum on the PR between 3 and 2 km, consistent with the melting of the hail and the narrowing of the size distribution;
- the presence of a differential polarization signal seen by S-POL radar extending from just below the 0°C level at 5 to 2.5 km, consistent with the occurrence of horizontally oriented oblate water-coated melting hail and nearly complete melting near 2.5 km;
- peak reflectivity of 50 dB*Z* at the 5-km level and a maximum rain rates of the 124 mm h^{-1} and concentrations of 4.2 g kg^{-1} at the surface from the melt water, thus indicating approximately the same concentrations of ice aloft.

These data are remarkably similar to the initial conditions of the Srivastava (1987) model of a microburst due to melting hail. In particular, for conditions very similar to those in the present case he finds the following.

- A small size hailstone (0.7-cm diameter) melts more rapidly at high relative humidity than at low RH due to the condensation on, and heat transfer to, the cold (0°C) melting ice. Complete melting occurs in 3 km of fall at RH = 70%, but half the mass melts in the last 0.7 km of fall (at a lapse rate of 7 K km^{-1}).
- For this reason the net cooling and negative buoyancy is concentrated in a narrow layer just above the height of final melting; an exponential distribution of small hail (with initial precipitation mixing ratio of 3.9 g kg^{-1} and reflectivity of 49 dB*Z*) melts in 2 to 3 km of fall in 300 to 400 s and produces a downdraft of 11 m s^{-1} at corresponding heights, almost exactly that found above from the profiler observations.
- The similarity between the present observations and the theoretical results of the Srivastava model results is striking and strongly supports the validity of the model. We suggest that wet microbursts, such as treated here, are favored by the presence of *small* hail or graupel that can melt aloft to produce the required negative buoyancy. The narrower the distribution of hail particle sizes, the more confined will be the layer of melting and negative buoyancy and the more intense the microburst. Increasing the mass loading also enhances the strength of the microburst. The occurrence of the microburst near the back of the storm cell where the cooling effect is maximized in relation to the warm ambient air suggests that this is a likely region for such events.

Finally, one cannot help but note the awesome value of the combination of the profiler, the dual Doppler radars, and the S-POL radar in providing the microphysics and kinematics of the storm. We have come a very long way since the 1946–47 days of the Thunderstorm Project (Byers and Braham 1949).

Acknowledgments. Drs. Atlas and Ulbrich are most appreciative of the support by NSF under Grant ATM 0223636, Atlas also acknowledges continued support under the Tropical Rainfall Measuring Mission (TRMM) and the hospitality of NASA Goddard Space Flight Center. Dr. Williams' participation was supported in part by NASA Grant NAG5-9753 under the TRMM program. We are deeply indebted to Prof. R. C. Srivastava of the University of Chicago for inspiring discussions without which this work could not have been done. We also thank Prof. Steven Rutledge and Dr. Rob Cifelli of Colorado State University (CSU) for data and insightful comments. We are grateful to Andrea Williams, formerly of CSU for Fig. 5; to Prof. V. N. Bringi of CSU for important comments and the measurement of the rain properties by the S-POL radar; to Tom Rickenbach of the Joint Center for Earth Systems Technology, University of Maryland, Baltimore, for useful discussions; and to Wen-Chau Lee of NCAR for calculations of the field of motion in the vertical planes. We also acknowledge the helpful suggestions of the reviewers and appreciate their complimentary remarks.

REFERENCES

Atlas, D., and C. W. Ulbrich, 2000: An observationally based conceptual model of warm oceanic convective rain in the Tropics. *J. Appl. Meteor.*, **39,** 2165–2181.

——, and C. R. Williams, 2003a: The anatomy of a continental tropical convective storm. *J. Atmos. Sci.*, **60,** 3–15.

——, and ——, 2003b: Radar echoes from lightning and their microphysical environment. *Geophys. Res. Lett.*, **30,** 1262, doi: 10.1029/2002GL016521.

——, R. C. Srivastava, and R. Sekhon, 1973: Doppler radar characteristics of precipitation at vertical incidence. *Rev. Geophys. Space Phys.*, **11,** 1–35.

Battan, L. J., 1964: Some observations of vertical velocities and precipitation sizes in a thunderstorm. *J. Appl. Meteor.*, **3,** 415–420.

Beard, K. V., 1976: Terminal velocity and shape of cloud and precipitation drops aloft. *J. Atmos. Sci.*, **33,** 851–864.

Bringi, V. N., and V. Chandrasekar, 2001: *Polarimetric Doppler Weather Radar: Principles and Applications.* Cambridge University Press, 648 pp.

——, G.-J. Huang, V. Chandrasekar, and E. Gorgucci, 2002: A methodology for estimating the parameters of a gamma raindrop size distribution model for polarimetric radar data: Application to a squall-line event from the TRMM/Brazil campaign. *J. Atmos. Oceanic Technol.*, **19,** 633–645.

Byers, H. R., and R. R. Braham Jr., 1949: *The Thunderstorm.* U.S. Govt. Printing Office, 287 pp.

Douglas, R. H., 1964: Hail size distribution. Preprints, *11th Weather Radar Conf.*, Boulder, CO, Amer. Meteor. Soc., 146–149.

Fujita, T. T., 1985: The downburst. SMRP Research Paper 210, University of Chicago, 122 pp. [NTIS PB-148880.]

Hu, Z., and R. C. Srivastava, 1995: Evolution of raindrop size distribution by coalescence, breakup, and evaporation: Theory and observations. *J. Atmos. Sci.*, **52,** 1761–1783.

Proctor, F. H., 1988: Numerical simulations of an isolated microburst. Part I: Dynamics and structure. *J. Atmos. Sci.*, **45,** 3137–3160.

——, 1989: Numerical simulations of an isolated microburst. Part II: Sensitivity experiments. *J. Atmos. Sci.*, **46,** 2143–2165.

Rasmussen, R. M., and A. J. Heymsfield, 1987a: Melting and shedding of graupel and hail. Part II: Sensitivity study. *J. Atmos. Sci.*, **44,** 2764–2782.

——, and ——, 1987b: Melting and shedding of graupel and hail. Part I: Model physics. *J. Atmos. Sci.*, **44,** 2754–2763.

Rickenbach, T. M., R. N. Ferreira, J. B. Halverson, D. L. Herdies, and M. A. F. Silva Dias, 2002: Modulation of convection in the southwestern Amazon basin by extratropical stationary fronts. *J. Geophys. Res.*, **107** (D20), 8040, doi:10.1029/2000JD000263.

Srivastava, R., 1987: A model of intense downdrafts driven by the melting and evaporation of precipitation. *J. Atmos. Sci.*, **44,** 1752–1773.

Stith, J. L., J. E. Dye, A. Bansemer, A. Heymsfield, C. A. Grainger, W. A. Peterson, and R. Cifelli, 2002: Microphysical observations of tropical clouds. *J. Appl. Meteor.*, **41,** 97–117.

Vivekanandan, J., V. N. Bringi, and R. Raghavan, 1990: Multiparameter radar modeling and observations of melting ice. *J. Atmos. Sci.*, **47,** 549–563.

Wakimoto, R. M., 2001: Convectively driven high wind events. *Severe Convective Storms, Meteor. Monogr.*, No. 28, Amer. Meteor. Soc., 255–298.

——, and V. N. Bringi, 1988: Dual-polarization observations of microbursts associated with intense convection: The 20 July storm during the MIST Project. *Mon. Wea. Rev.*, **116,** 1521–1539.